Aspects of goethite surface microtopography, structure, chemistry, and reactivity

JOHN RAKOVAN,* UDO BECKER,† AND MICHAEL F. HOCHELLA JR.

Mineral Surface Sciences Laboratory, Department of Geological Sciences, Virginia Polytechnic Institute and State University, Blacksburg, Virginia 24061, U.S.A.

ABSTRACT

Goethite (010), (110), and (111) growth faces and (010) cleavage surfaces of large, natural single crystals, as well as a high surface area synthetic sample were characterized using various surface sensitive microscopies and spectroscopies. Differential interference contrast and atomic force microscopy characterization of the natural single crystal faces showed microtopography indicative of growth, dissolution, and cleavage. Low energy electron diffraction patterns of the goethite (010) surface exhibit sharp, intense diffraction spots, indicating long-range order on this important surface. These patterns have two-dimensional point group symmetry $2mm$, consistent with an undistorted surface structure and unit-cell parameters $a = 4.62 \pm 0.14$ Å and $c = 2.99 \pm 0.08$ Å. These parameters equal the equivalent bulk cell dimensions given the uncertainties. Ultra-high vacuum scanning tunneling microscopy was performed on (010) cleavage faces, although the tunneling properties of the surface were very heterogeneous. Atomic resolution was not obtained; however, microtopographic images are identical to those collected with AFM. XPS spectra from the (010) faces of two natural samples as well as the synthetic powder all have peak maxima for Fe ($2p_{3/2}$) at 711.5 ± 0.1 eV. The O($1s$) line originating from the goethite can be fit with two peaks with a chemical shift of 1.3 eV. The peak at higher binding energy (531.3 eV ± 0.1 eV) represents the protonated oxygen in the structure, and the peak at lower binding energy (530.0 eV ± 0.1 eV) represents the proton-free oxygen in the structure. Ab initio and semi-empirical models of the (010) surface suggest that cleavage occurs through the hydroxide plane at $1/4\ b$ in the structure. This is contrary to cleavage through the oxide plane at $1/2\ b$, which has been assumed in several previous studies.

INTRODUCTION

The surface structure and composition of a mineral play a pivotal role in the chemical interactions that take place between that mineral and its environment. Sorption and desorption behavior, catalytic reactivity, and growth and dissolution mechanisms are all determined by surface structure and composition. Unfortunately, the definitions of these surface characteristics are not as straight forward as one might initially assume. The term "surface structure" has been used to denote everything from surface topography, described in scales from centimeters down to nanometers, to the local atomic structure around one particular site on a crystal surface. The thickness of the uppermost layer defined as the "surface" varies and is often determined by the resolution of the particular analytical technique used. For example, scanning probe microscopes (SPM) generally probe the top-most layer of atoms only, whereas X-ray photoelectron spectroscopy (XPS) typically has an analytical depth of a few tens of angstroms. Yet, all of the structural and compositional attributes of a mineral's surface are probably important in understanding its functionality in nature, from macroscopic to microscopic scales.

A large literature dealing with goethite surface chemistry already exists (see Cornell and Schwertmann 1996 and references therein), yet intriguing questions remain, especially involving surface structure and reaction heterogeneity. These aspects of the surface chemistry of goethite are particularly important to soil science because goethite is the most abundant iron oxide. Although its absolute abundance in a soil may be only between 1 and 5%, goethite surfaces may account for 50 to 70% of the total surface area of the soil as a whole (Schwertmann and Taylor 1990). This is due both to the small size of soil goethite crystals [commonly acicular crystals 10 and 100 nm in length with surface areas of 60–200 m^2/g (Schwertmann and Taylor 1990)], and to goethite forming coatings on larger soil grains. Furthermore, because goethite has a high affinity for sorption of many cations and anions (Cornell and Schwertmann 1996), it is thought to be a major player in the cycling and retention of geochemically and environmentally important elements such as heavy metals. In this paper, various aspects of both the structural and compositional nature of growth and cleavage surfaces of goethite are described, with observations encompassing a wide range of scales from optical resolution down to the atomic level.

A wide variety of analytical techniques are combined to characterize surface microtopography, composition, and atomic structure for goethite. X-ray photoelectron spectroscopy (XPS) was used for surface compositional analysis. Low energy electron diffraction (LEED) provides information on the long-range atomic order of a surface (e.g., Hochella 1990), and quantum mechanical modeling (Crystal95 and a procrystal model) provide short-range information on local atomic surface configurations (e.g., Becker and Hochella 1996; Becker et al. 1996).

*Present address: Department of Geology, Miami University, Oxford, OH 45056, U.S.A. E-mail: Rakovajf@muohio.edu
†Present address: Institut für Mineralogie, Universität Münster, Corrensstrasse 24, D-48149, Münster, Germany.

Together, these two methods give insights into surface atomic structure and its role in surface reactivity on different crystal faces. Differential interference contrast (DIC) microscopy is used to characterize surface topography from macroscopic scales down to the micrometer range in terms of lateral spatial resolution. At this point, atomic force microscopy (AFM) becomes most useful, allowing observations of these same features down to the nanometer scale. Thus, DIC and AFM used in concert provide for a useful and complimentary range of scale coverage for the observation of growth and/or dissolution mechanisms operative on a particular face. Microtopographic observations can give insight into the type and number of chemically active sites on that surface (Sunagawa 1987a; Rakovan and Reeder 1996; Junta-Rosso et al. 1997).

Of the techniques listed above, DIC, XPS, and LEED do not have the lateral resolution to use on soil goethites with sizes well into the submicrometer range. Therefore, we used primarily large single crystals of goethite of hydrothermal origin in this study. Crystal growth faces and large (010) cleavage planes of the hydrothermal goethites were studied. The rationale is that cleavage plane characteristics are independent of the crystal size and thus germane to soil samples. Furthermore, the degree of surface alteration on natural samples is unknown and cleavage planes present pristine surfaces. Finally, we have chosen a high surface area synthetic goethite to compliment the natural specimens in the XPS portion of this study.

EXPERIMENTAL METHODS

Samples

The single crystals are from Pikes Peak, Colorado, (National Museum of Natural History, Smithsonian Institution no. 152060) and Cornwall, England (Harvard Mineralogical Museum no. 83826 and no. 96672). The Colorado sample is an aggregate of intergrown bladed crystals with lengths up to 3 cm and widths up to 1 cm. These crystals are dominated by the {010}. The samples from Cornwall include single crystals with lengths up to 5 mm and widths up to 2 mm with well-developed euhedral morphology and multiple forms including the {110}, {010}, {120}, {111}, and {101} (Fig. 1). For both samples, crystal faces were indexed by goniometric measurements. Cleavage surfaces generated from these crystals are parallel to the (010) indexed growth faces as expected, and LEED patterns taken from these cleavage surfaces are consistent with a (010) termination.

Samples of fine-grained synthetic goethite with a surface area of 85 m^2/g, determined by BET analysis, were prepared from ferrous sulfate in a 1 N bicarbonate solution according to the recipe in (Schwertmann and Cornell 1991). X-ray diffraction showed no other iron oxide in the synthetic samples. The morphology of these crystals is undetermined.

In general, microcrystalline soil goethites are dominated by the (110) form (e.g., Cornell and Schwertmann 1996) but other forms may be present. Large hydrothermal goethites, such as those in this study (Fig. 1) tend to be morphologically more complex.

Differential interference contrast microscopy

Optically visible microtopography of growth and cleavage surfaces was photographically recorded using DIC microscopy
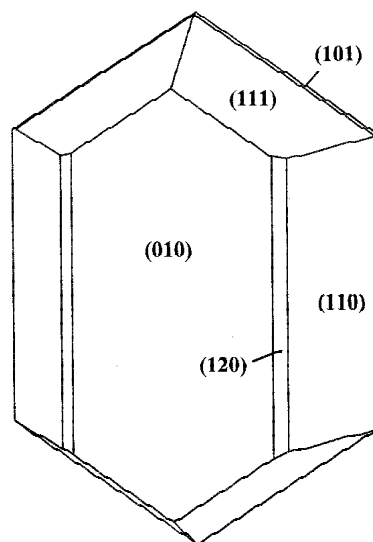

FIGURE 1. Schematic of the morphology of a single goethite crystal from Cornwall, England.

on a Nikon Optiphot petrographic microscope. In DIC a polarized beam of light is split by a Wollaston prism into two beams, which are reflected by a sample surface. Surface microtopography leads to phase differences in the reflected wave fronts. The reflected beams are then recombined as they pass back through the prism and then through the analyzer. Because of the phase shift between the two beams, recombination and transmission through the analyzer leads to interference colors that vary between regions of the surface with different orientations, thus enhancing their contrast and detection. Although DIC can detect height differences of a few angstroms (Sunagawa 1987a), its lateral resolution is limited to the wavelength of the illuminating light (roughly 0.5 μm).

Scanning probe microscopy

Quantitative measurements of surface microtopography were made on a Digital Instruments Nanoscope III AFM in contact mode using standard silicon nitride tips. As-grown crystal surfaces were cleaned by sonification in a soap solution and rinsed in multiple cycles of deionized water and ethyl alcohol. Residual water from the final rinsing was removed by blowing the sample dry in a stream of N$_2$. Cleavage surfaces were freshly prepared with a scalpel and vigorously dusted with a stream of N$_2$. Crystals were mounted on sample stubs with colloidal carbon suspended in alcohol (DAG) and observed in air on the AFM. All AFM images were collected in height mode so that quantitative measurement of the surface relief was possible. In the configuration used here, AFM has angstrom-scale vertical resolution with a 3 μm z-range, and nanometer-scale horizontal resolution.

Scanning tunnelling microscopy (STM) data were collected on cleavage surfaces in ultra-high vacuum (UHV) using an Omicron UHV STM-1 mounted on an Omicron UHV Compact Lab. Electrochemically etched tungsten and mechanically cut Pt/Ir STM tips were used. Samples were cleaved in air and put into the vacuum chamber within 30 min. Base pressures ranged from

1×10^{-9} to 10^{-11} Torr. For all samples, tunneling was achieved with some difficulty even though goethite is a semiconductor with a band gap of 2.1 eV (Leland and Bard 1987). This is similar to that of hematite (2.2 eV) where tunneling is much more routine (e.g., Eggleston and Hochella 1992). Tunneling currents were set in the vicinity of a few nanoamps and bias voltages from 2.2–8 V.

X-ray photoelectron spectroscopy

A Perkin-Elmer 5400 XPS system was used. Before XPS analysis, samples were exposed to evaporated gold in a coater for 1 s so that binding energies could be calibrated using the $Au(4f_{7/2})$ peak at 84.0 eV. AlK X-radiation was used at a power between 200 and 300 watts. Base pressures were lower than 5×10^{-8} Torr. Survey scans were collected to 1000 eV binding energy using 1 eV steps of 20 ms per step counting time, and a detector pass energy of 89.45 eV. Collection time for survey scans was 10 min. High-resolution narrow scans ranged from 10 to 50 eV windows widths using 0.1 eV steps of 50 ms per step and a detector pass energy of 17.55 eV. Spectra taken from the Cornwall and Colorado samples were from large pristine (010) cleavage surfaces. Spectra were fit using a Microsoft Excel spreadsheet developed by H.W. Nesbitt, I.J. Muir, and A.R. Pratt of the University of Western Ontario. This software uses a Shirley background correction and Gaussian-Lorentzian peak fitting.

Scanning electron microscopy (SEM)

An ISI SX40 SEM was used to supplement DIC, AFM, and STM imaging. In conjunction with SEM imaging, energy dispersive X-ray spectroscopy (EDS) was used to help identify secondary phases on goethite growth surfaces. Samples were gold coated for SEM imaging and EDS analysis.

Low energy electron diffraction

An Omicron reverse view 4-grid LEED mounted on an Omicron UHV Compact Lab was used in this study to determine the crystallinity of (010) growth and cleavage surfaces. Instrument settings were calibrated with LEED patterns from the known (100) surface cell of galena (Hochella et al. 1989). The galena was fractured in vacuum and diffraction patterns were recorded at a range of energies from 20 to 135 eV. For goethite samples, surfaces were prepared as described in the AFM section above. Diffraction patterns were visible between 99 eV and 213 eV. Observed diffraction patterns did not fade in intensity over a period of roughly one half hour under these conditions. The best peak-to-noise ratio was achieved at around 113 eV.

The procrystal model

A modified version of SPEEDEN (a procrystal model) (Downs et al. 1996) was used to study the (010) surface of goethite. Before this procrystal model is described, the following background is helpful. Bader (1990) showed that bonding can be defined by the electron density distribution between two atomic centers. If a bond does exist between two atoms, then there must be an atomic interaction line or a continuous ridge of electron density between them. Along the bond path, the electron density decreases from each atomic center to the saddle point in between. The saddle in the electron density distribu-

tion along this interaction line is called a "(3,–1)" critical point. Such a point in the electron density is defined by a local maximum in the plane perpendicular to the interaction line and a minimum along the interaction line or bond path.

In the procrystal model, the electron density distribution of a crystal is approximated by superimposing spherically averaged (Gibbs et al. 1992) Roothan-Hartree-Fock wave functions (Clementi and Roetti 1974) expressed as linear combinations of Slater-type functions of non-interacting, neutral atoms in their ground state and located at the positions that they occupy in the crystal structure. From this, electron density distributions and critical points are determined, and bond paths are followed, leading to a quantitative understanding of bond location in the structure. The electron density distribution and critical points predicted by this model closely agree with experimental values (Gibbs et al. 1998).

Here, the procrystal model was used to generate the full bond topology and critical point properties of goethite. This in turn was used to determine the most favorable atomic plane parallel to (010) for cleavage because the electron density at these critical points is a measure of bond strength. Goethite structural parameters used in this calculation were taken from (Forsyth et al. 1968).

Crystal95

To derive surface energies for different surface terminations perpendicular to [010], we compared the total energies of goethite slabs that were infinite in size in the a-c plane and two unit-cells thick along b (two-dimensional periodic boundary conditions) with the total energy of bulk goethite (three-dimensional periodic boundary conditions). Total energies of a unit cell within the slab and bulk were calculated using Crystal95, an ab-initio molecular orbital program for periodic structure calculations (Pisani et al. 1988; Dovesi et al. 1992; 1996). This program introduces periodic boundary conditions by solving the coulomb integral and the exchange integral in reciprocal space. Calculations were performed by using a 3-21G Pople-type basis set with polarization functions on the O atoms. The slab surfaces were chosen to be structure terminations with no dipole moments perpendicular to the surface plane. The atomic positions on the slab surfaces were not allowed to relax from bulk positions because the energy to be applied during cleavage does not depend on the energy that is gained due to relaxation after cleavage. Total energies of the slab unit cell had to be divided by two because the slab thickness was twice the b dimension and the slab is terminated by an upper and a lower surface.

EXPERIMENTAL RESULTS AND DISCUSSION

Surface microtopography

DIC and SPM observations. DIC images showing the regional microtopography of the (010), (110), (111) growth surfaces of the Cornwall samples and a (010) buried growth surface of the Colorado sample are shown in Figures 2a–d. The (010) growth surfaces of the Cornwall goethites exhibit several growth and etch features. Very elongate hillocks with rounded macrosteps (Fig. 2a) dominate the microtopography as observed by DIC. The direction of elongation is always along [001]. The (111) faces of the Cornwall samples show complex microtopography
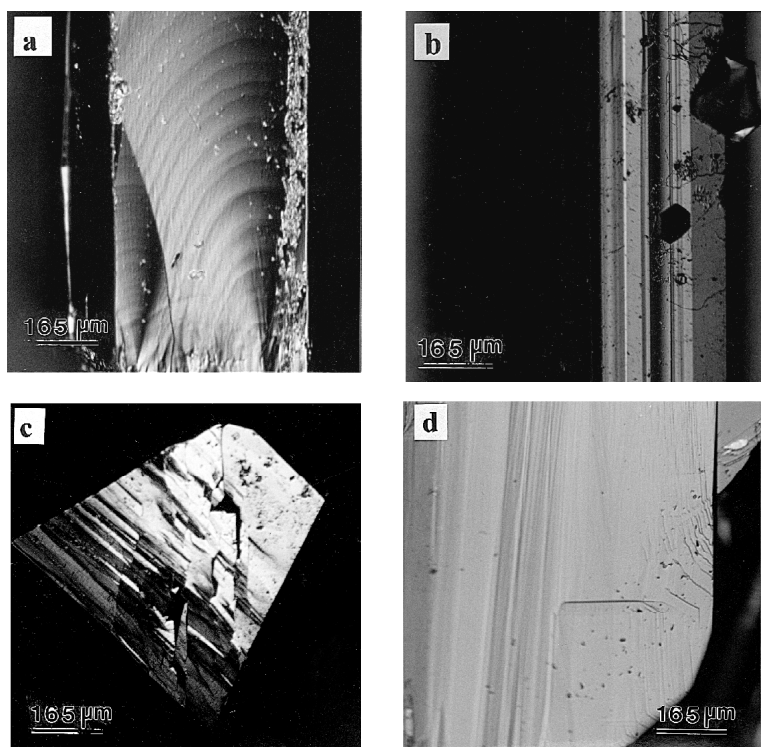
FIGURE 2. DIC photomicrographs of **(a)** a (010) face **(b)** a (110) face, and **(c)** a (111) face of a Cornwall goethite crystal and **(d)** a (010) buried growth surface on a Colorado, goethite crystal.
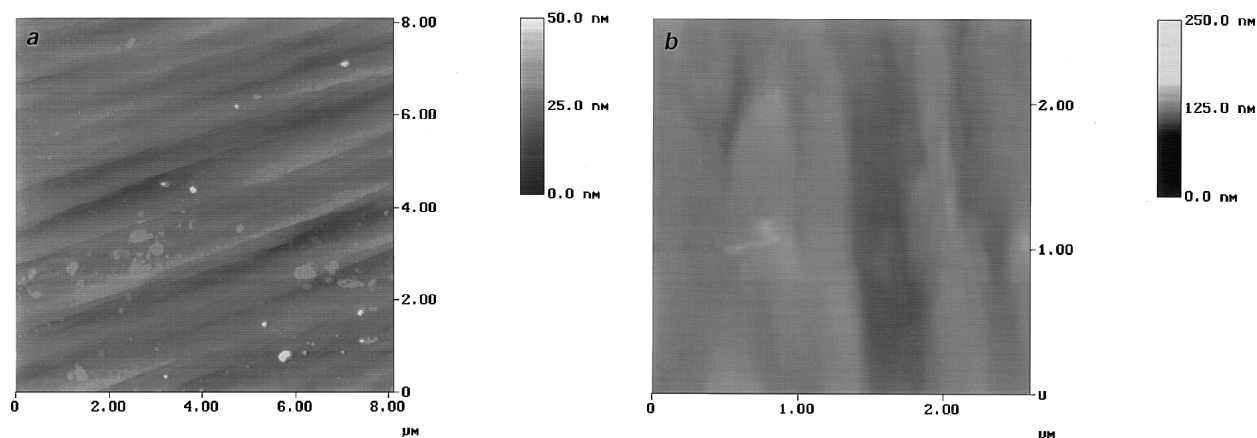

FIGURE 3. **(a)** AFM image in height mode of steps on the rounded, elongate (010) growth hillock in Figure 2a. **(b)** AFM image in height mode of small mounds on the rounded, elongate (010) growth hillocks in Figure 7a.

that may represent very asymmetric and rounded growth features such as hillocks (Sunagawa 1987b). The growth features exhibited by the (010) and possibly those on the (111) suggest that these faces grew by a spiral growth mechanism.

AFM images show two types of fine-scale morphologies on (010) growth surfaces. Macrosteps seen in DIC were also observed with AFM along with much smaller steps (striations) that were resolvable down to about 10 Å in height (Fig. 3a). Unlike cleavage steps, all of these features have no sharp step edges. This is typical of many other natural growth steps and striations that we have imaged on other minerals (i.e. barite, pyrite, catapleiite, graphite, and apatite). A second type of fine-scale microtopography was observed with AFM on some of

the (010) growth faces. This consisted of densely packed rounded mounds elongated in the [001] direction and 5 to 30 nm in height (Fig. 3b).

Splitting of the Colorado goethite crystals leads to the development of two distinctly different types of surfaces. The surface that is most often exposed when splitting the Colorado samples exhibits features similar to the growth surfaces (Figs. 2d and 4). These surfaces are uneven with many steps of different size and are plainly different from true cleavage surfaces described below. The Colorado sample is comprised of clusters of multiple-bladed crystals in parallel and divergent orientation and the distinct microtopography of this first type of surface suggests that they are buried growth surfaces or grain
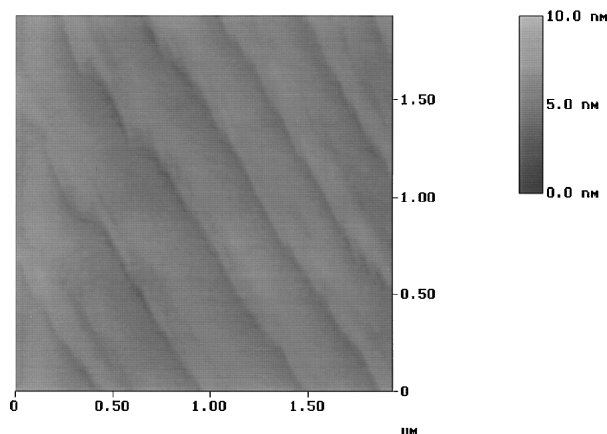
FIGURE 4. AFM image of parallel steps on an exposed buried growth surface of a Colorado goethite.

boundaries. The second type of surface exposed is an obvious cleavage surface with large flat terraces separated by cleavage steps of varying height (Fig. 5). The terraces are atomically smooth and cleavage steps vary in height from roughly 9.9 Å, the [010] unit-cell dimension, to multiples of this (Figs. 6a and 6b). The orientation and shape of the cleavage steps are variable, and are often curved (Fig. 6a). However, some cleavage steps have a polygonized shape (Fig. 6b). Such heterogeneities in the morphology of cleavage steps on a given cleavage face have been seen on other minerals and have been interpreted by Stipp et al. (1994) to be due to local differences in the stress regime as a fracture is propagating through the crystal.

The (110) surface and periodic bond chains. Surface microtopography can be indicative of the mechanism of growth on a given face (Sunagawa 1987a). In part, the type of growth mechanism that can operate on a crystal face is dictated by the atomic structure of that face. Periodic bond chain (PBC) theory predicts the possible growth mechanisms of a given face by analysis of the atomic structure of the surface slice parallel to that face (Hartman and Perdok 1953). A PBC is a structural sequence or chain of uninterrupted strong bonds within a structure. A crystal face can be categorized by the number of non-parallel PBCs within a slice parallel to that face. F faces contain two or more PBCs, S faces contain only one PBC, and K faces have no PBCs. In Hartman and Perdok's PBC theory, only F faces should grow by a spiral mechanism. The growth rate of F faces is predicted to be slower than that of S and K faces, hence F faces should dominate the crystal habit. One possible manifestation of spiral growth is the formation of growth hillocks, such as those observed on the (010) growth surfaces of the goethite samples from Cornwall (Figs. 2a and 7a). S faces on the other hand typically show steps of one orientation only, hence they may have a striated microtopography such as that on the (110) of goethite (Fig. 2b). S-type faces may form by the pile up of growth steps along the edges of adjacent F faces that grow by a layer mechanism (Sunagawa 1987b). If this is the case for the (110) of goethite it would not be expected that it would grow to such a large size. Rakovan and Reeder (1994) have shown that the (100) faces of apatite, which are usually strongly striated in one direction, may grow by a spiral mechanism and develop polygonized growth hillocks. Both the presence of such growth hillocks and the re-

sults of a periodic bond chain analysis for apatite (Terpstra et al. 1986) indicate that the (100) is an F-face by the criteria of Hartman and Perdok (1953) but may also develop surface microtopography predicted for S-type faces. The development of unidirectional striations rather than hillocks may depend on the exact conditions of growth. This may also be the case for the (110) faces on goethite.

Layer growth shadows. Surface pits of several different morphologies have been observed on different Cornwall samples superimposed on the growth features of the (010) faces. The first type of pit is rectangular and strongly elongate along [001]. The shape of these pits reflects the 2mm symmetry of the (010) face and is inferred to be due to etching (Fig. 8). The width of these pits is between 5–25 mm with a depth of 10–70 nm and therefore they are best observed with the AFM. The second type of pit is triangular, strongly asymmetric and does not reflect the surface symmetry of the (010) face (Fig. 7). The fact that these are depressions and not raised features was determined by AFM. We believe that these pits are not etch features, but rather are formed by a "layer growth shadow" on the surface. At the base of all of these triangular pits is a depression with a morphology that appears to be a cast of a relict crystal. The apices of the triangular pits point in the direction of growth step advancement which is inferred from the morphology of the hillocks. The aspect ratio and asymmetry of the pits are related to the orientation of the inclusion casts. Where the long axis of a relict inclusion is roughly perpendicular to the direction of step advancement the associated triangular depression exhibits symmetric development of its two flanks. The aspect ratio of these pits is also relatively low. Where the long axis of a relict inclusion is highly inclined to the direction of step advancement (i.e., 30°) the associated triangular depression has a much higher aspect ratio. They are less symmetric with greater development of the pit wall associated with the end of the inclusion that was pointing in the opposite direction of step advancement. Also, AFM observations of the fine-scale microtopography along the walls of these pits show scale-like
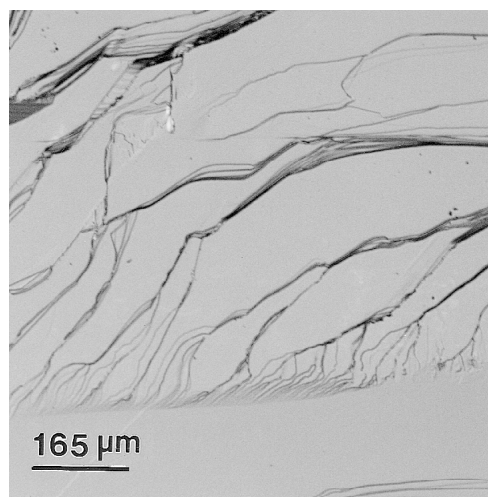

FIGURE 5. DIC photomicrograph of an (010) cleavage surface on a Colorado goethite.
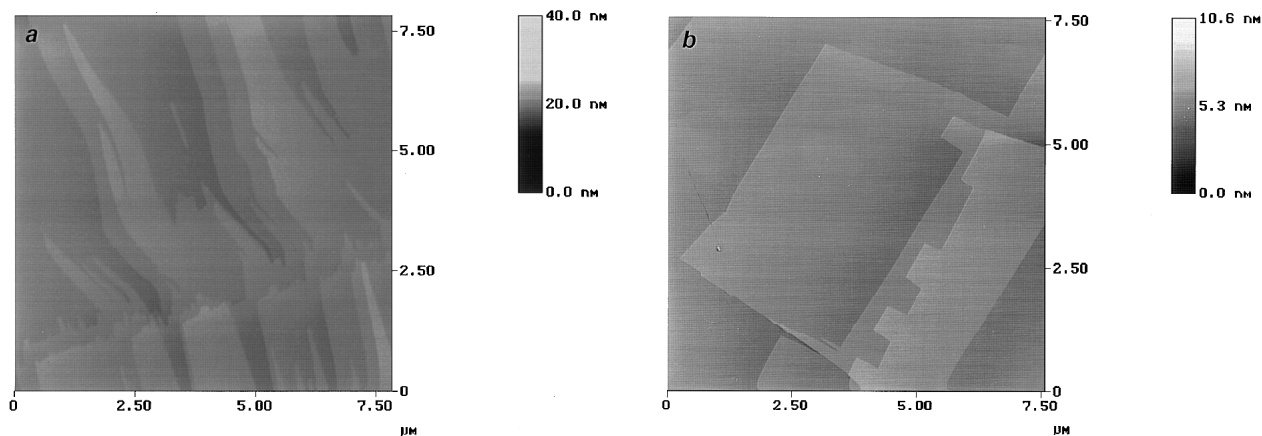
FIGURE 6. AFM images in height mode of (010) cleavage surface on a Colorado goethite. **(a)** Curved steps. **(b)** Polygonal steps.

growth features that are identical to the microtopography observed along raised growth features on the same face (Fig. 3b). We suggest that these depressions formed as migrating growth steps encountered the preexisting inclusion phase. The surface inclusion shadowed the region behind it from the advancing steps creating a depressed area relative to adjacent regions that were not shadowed by the surface inclusion. Such surface depressions are ideal for the entrapment of fluid inclusions as growth continues. The association of fluid inclusions and solid phase inclusions in crystals is often used as an indication of the primary nature of the fluid inclusion (Roedder 1984; Yang and Bodnar 1994), and "layer growth shadows" may be one mechanism for their formation.

UHV STM was conducted on large (3 mm × 3 mm) cleavage surfaces of the Colorado goethite specimens with the hope of obtaining atomically resolved surface images. Although tunneling to the goethite sample was achieved, the desired atomic scale images were not. Tunneling properties were very heterogeneous over these surfaces. This may be due to the presence of contamination phases present along the interface of buried growth surfaces within the crystal fragments, and the fact that these fragments may not have been strictly single crystals but aggregates of bladed crystals in parallel growth. Evidence for insulating phases on buried growth surfaces is given in the surface composition section below. Nevertheless, regional microtopographic images (1 μm × 1 μm and larger) were ob-

tained with STM and showed surface cleavage features identical to those observed by AFM.

Morphological comparison with other AFM studies. Several studies have looked at the morphology and surface microtopography of microscopic, synthetic goethite crystals (Fischer et al. 1996; Weidler et al. 1996; Barrón et al. 1997). Weidler et al. (1996) showed crystals that are dominated by the (110) and (100) and terminated by the (021). The surface microtopography of the (100) is dominated by growth steps that are similar in their distribution to those seen on the (010) of the sample in Figure 2a. Weidler et al. (1996) used interfacial angles to index the faces on their samples; however, these angles are not reported. Barrón et al. (1997) has shown that indexing of the (021) is in error. The measured angle between the (110) and the (021) faces actually reflects the angle of the tip faces and not that of the crystal. The supposed (021) faces on Barrón et al. (1997) samples were also observed when measuring with silicon nitride tips. However, they disappeared when the same crystals were scanned with higher aspect ratio silicon tips.

Surface chemistry

Photoelectron peak assignments and positions. $Fe(2p_{3/2})$ peaks (Fig. 9) are wide and asymmetric due to multiplet splitting and were fit using four components calculated by Gupta and Sen (1974). The four peaks were constrained to be separated by 1.00, 2.20, and 3.55 eV and the peak height ratios
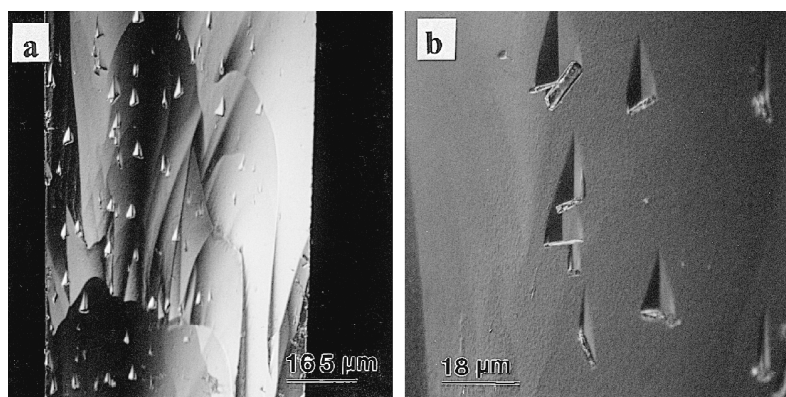

FIGURE 7. DIC photomicrographs of the (010) growth surface of a Cornwall, goethite. **(a)** 200× view of rounded, elongate growth hillock with triangular pits. **(b)** 400× view of triangular pits and casts from relict surface inclusions.
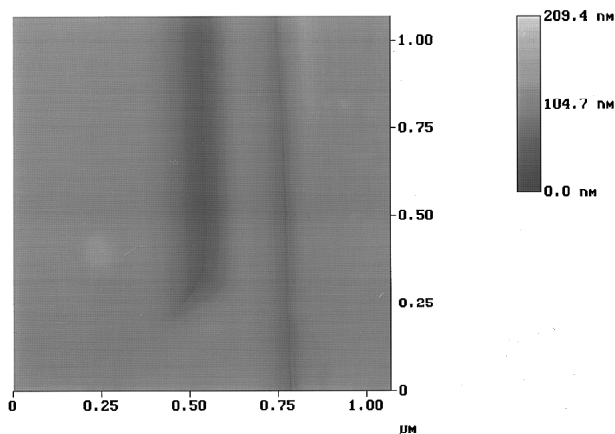
FIGURE 8. AFM image in height mode of elongate, rectangular etch pits on the (010) growth surface of a Cornwall, goethite crystal.

relative to the lowest binding energy peak were constrained to be 0.95, 0.59, and 0.28 (Pratt et al. 1994). O(1s) peaks from the goethite (Fig. 9) were fit with two components for the synthetic sample and four components for the natural samples, and the assignments for structural O^{2-} and OH^- peaks are well established in the literature (e.g., Junta and Hochella 1994). Photoelectrons from the structural O^{2-} at 530.0 eV and the structural OH^- at 531.2 to 531.3 eV make up 70 to 80% of the area of the O(1s) peak envelope for the natural samples. The smaller high-binding energy lines for these samples can be precisely accounted for by photoelectrons from the Al sample stub at 532.3 eV and colloidal carbon (DAG) at 533.0 eV. These exact binding energies were confirmed by collecting spectra of the Al stub and DAG without the sample.

A comparison of $Fe(2p_{3/2})$ and O(1s) binding energies measured in this study vs. those measured in other studies is given in Table 1. Our $Fe(2p_{3/2})$ binding energies for goethite match those of Welsh and Sherwood (1989) and Junta-Rosso and Hochella (1996). McIntyre and Zetaruk (1977) and Harvey and Linton (1981) have line positions about 0.5 eV higher and lower than our energy, respectively, but these studies used adventitious C to calibrate their energies, and this method is known to be only approximate (Stipp and Hochella 1991). The $Fe(2p_{3/2})$ binding energy for goethite derived by Brundle et al. (1977) is almost within the error of our number if their Au calibration energy is adjusted to the more typically used value of 84.0 eV. Why the binding energy determined by Allen et al. (1974) is so
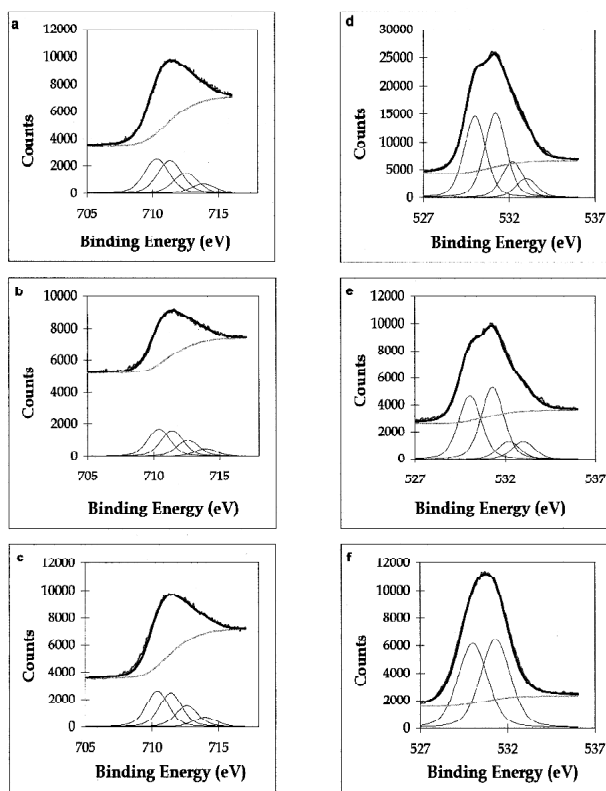

FIGURE 9. XPS spectra of the Fe (2p3/2) core region and O (1s) peaks for the Cornwall (**a** and **d**), Colorado (**b** and **e**), and synthetic goethites (**c** and **f**). Spectra form the Cornwall and Colorado samples were collected from the (010) cleavage surfaces. Crosses = datapoints. Grey line = baseline. Light solid lines = component peaks. Heavy solid line = sum of the compents and the baseline.

low is not known. Nevertheless, we believe that the $Fe(2p_{3/2})$ binding energy for goethite at between 711.4 and 711.5 eV can be considered to be a definitive value. That this energy is approximately 0.5 eV higher than that measured for hematite (Junta-Rosso and Hochella 1996) is expected. The Fe-OH bonding in goethite, vs. only Fe-O bonding in hematite, results in reduced shielding on the iron core, slightly increasing the binding energy of iron core lines. A similar effect was observed in C(1s) binding energies between CO_3 and CO_3H groups on the surface of calcite (Stipp and Hochella 1991).

TABLE 1. XPS $Fe(2p_{3/2})$ and O(1s) binding energies

Fe(2p3/2)	O(1s)-oxide	O(1s)-hydroxide	Sample charge reference	Reference
711.5*	530.1	531.3	Au 4f7/2 at 84 eV	This work†
711.4*	530.0	531.2	Au 4f7/2 at 84 eV	This work‡
711.5*	530.0	531.3	Au 4f7/2 at 84 eV	This work§
711.9	NR‖	NR‖	C1s	(McIntyre and Zetaruk 1977)
711.0	530.1	531.8	Au 4f7/2 at 84 eV	(Allen et al. 1974)
711.4	530.3	531.5	O1s at 530.3 eV	(Welsh and Sherwood 1989)
711.2	530.1	531.1	Au 4f7/2 at 83.95 eV	(Brundle et al 1977)
711.4	NR	NR	O^{2-} O1s at 530.0 eV	(Junta-Rosso and Hochella 1996)
711.0	529.6	530.9	Referenced to C1s at 284.6 eV	(Harvey and Linton 1981)

* Peak maximum determined by a weighted average (with respect to peak area) peak position obtained from a four component fit spectra.
† Cornwall, England.
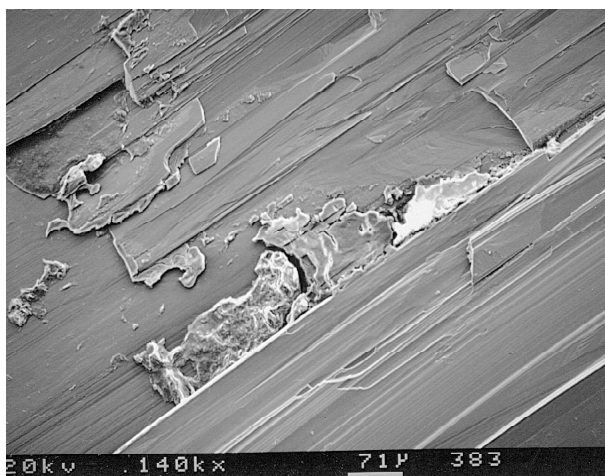‡ Pikes Peak, Colorado.
§ Synthetic.
‖ Not reported.

FIGURE 10. SEM photomicrograph of buried growth surfaces on a Colorado goethite.

McIntyre and Zetaruk (1977) compared XPS spectra of hematite and goethite. They note that the nonprotonated structural O(1s) peak of goethite is shifted 0.5 ± 0.1 eV to higher binding energy relative to that in hematite and suggest that it reflects interactions between the proton on the OH group and the nonprotonated oxygen across the [001] channels (Pbnm setting) of the goethite structure. The results of our procrystal calculations of the electron density in the goethite structure (see below) are consistent with a weak hydrogen-nonprotonated oxygen interaction that may be responsible, at least in part, for this observed chemical shift.

Surface composition. If the goethite crystals used in this study are stoichiometric, then O and OH must be found in equal quantities in the structure. Yet, fitted O(1s) spectra (Fig. 9) consistently show a slightly more intense OH peak relative to the O peak. The intensity proportion for the three spectra shown is 52% OH and 48% O, $\pm 1\%$. Considering the XPS depth of analysis in terms of photoelectron escape depth (Hochella 1988b), and the escape depth for metal oxides at the kinetic energy of O(1s) photoelectrons ejected by AlKa X-rays (Hochella and Carim 1988a), we can estimate that approximately 20% of the O(1s) signal comes from the top 5 Å of these samples. Next, considering the atomic structure of goethite on the (010) surface and sampling depth in the [010] direction (see next section for more details on structure), we calculate that a fully hydroxylated top monolayer of O atoms would result in the same 52% OH, 48% O intensity ratio observed. This observation is important when discussing the atomic structure of the uppermost surface of goethite (010) in the next section.

XPS survey scans of freshly exposed buried growth surfaces in the Colorado goethites occasionally showed the presence of minor amounts of Si, Al, and Mg. SEM was used to look for other phases along these buried surfaces. Figure 10 is an SEM image of a freshly exposed buried growth surface. In the center of the image are several anhedral masses. EDS analysis shows these to be K, Mg, Al silicate phase(s), which accounts for the presence of these elements in some of the XPS spectra. No such inclusions were found in the Cornwall samples. Considering that the Cornwall samples are single, euhedral crys-
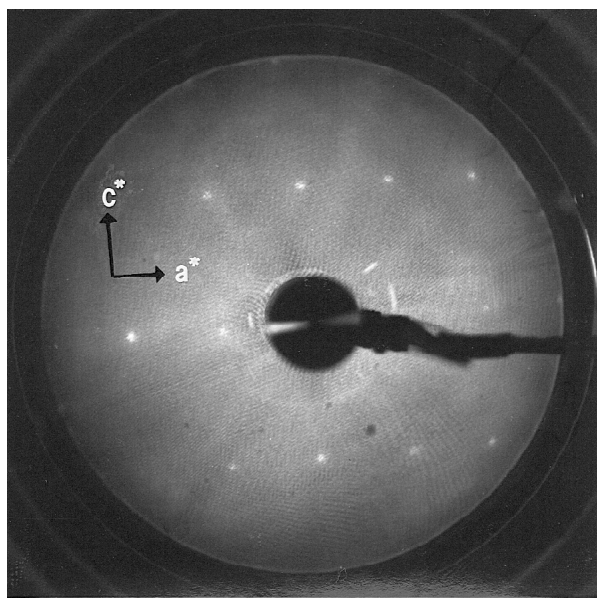

FIGURE 11. LEED pattern from the (010) of the Colorado goethite.

tals with no internal grain boundaries, this is not surprising.

Surface structure on (010)

The atomic surface structure of goethite is not well known. In part, this may be due to the difficulty of surface structural analysis on very small crystals. Experimentally, goethite surface structures were studied by spectroscopic (IR and XAS) evaluation of adsorbed species such as phosphate, selenate, and selenite (Russell et al. 1974, 1975; Parfitt et al. 1975; Hays et al. 1987; see also Sposito 1984). It is assumed that goethite surfaces are made up of various proportions of A-, B-, and C-type sites, which are surface O atoms (or hydroxyls) coordinated to 1, 2, or 3 Fe atoms (Russell et al. 1974; Russell et al. 1975) designated monodentate, bidentate, and tridentate sites, respectively. Sposito (1984) argues that the A-site is amphoteric, that is it can gain or lose a proton, and that B- and C-sites are unreactive. Below, we present the first published LEED measurements for goethite, as well as modeling results that give insight into the specific structure of the (010) surface.

LEED results. LEED patterns of the (010) cleavage and buried growth surfaces of crystals from Colorado (Fig. 11) show sharp intense spots indicating an atomically well-ordered surface, and the diffraction patterns do not degrade with time indicating a stable surface structure even under electron beam bombardment. The plane group symmetry is *2mm* as would be predicted for a simple truncation of the bulk structure on the (010). Surface cell measurements were calculated from eight individual photographs and averaged. The measured (010) surface unit-cell dimensions are $a = 4.62 \pm 0.14$ Å and $c = 2.99 \pm 0.08$ Å. These are within experimental error of the equivalent bulk unit-cell dimensions of 4.59 Å and 3.02 Å.

To remove adventitious material from the surface, the sample was heated in vacuum to 130 ºC for 5 min. After heating no LEED pattern was observed, due to loss of long range order at the surface, which may be the result of heterogeneous surface
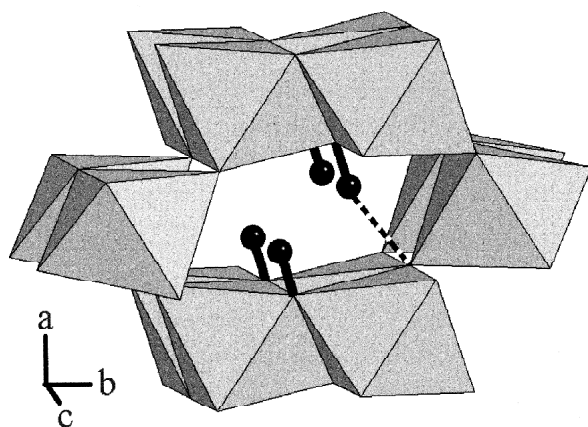
FIGURE 12. Schematic of a segment of the goethite structure. Polyhedra represent Fe in octahedral coordination. Balls represent H atoms. Solid lines show O2-H bonds and the dashed line indicates an O1-H bond.

dehydroxylation. Bulk dehydroxylation occurs in air at roughly 320 °C for well-crystallized goethite (Schwertmann 1984), but dehydroxylation of the surface may occur at a much lower temperature in vacuum.

The bulk structure of goethite and possible (010) surfaces. Although the LEED results show that the (010) surface has long-range atomic ordering with symmetry that is consistent with the bulk structure perpendicular to the *b* axis, it does not tell us where along the *b* axis this plane intercepts. In fact, there are only two planes perpendicular to *b* that have no dipole moments perpendicular to the surface plane, and therefore cleavage presumably occurs along one of these planes. A brief review of the bulk structure of goethite is given next before discussing these two possibilities.

The bulk goethite structure consists of double rows or ribbons of edge-sharing Fe octahedra which parallel [001] and are two octahedra wide along [010] (Fig. 12). Octahedral ribbons are separated along [010] and [100] by vacant double rows or "pseudo-channels" that also run along [001]. The ribbons are connected to one another by sharing of apical oxygen atoms at their edges.

The first possible (010) cleavage plane is located at 1/2 *b*. This plane is defined by O1 atoms that reside just above and below it. If breakage occurs along this plane, half of the O1 atoms go to one side and half go to the other side. Along this plane, two O1-Fe bonds must be broken per (010) surface unit cell. The second possible plane is located at 1/4 *b*, and is defined by O2 atoms, all part of hydroxyl groups, located just above and below the plane. If breakage occurs along this plane, half of the O2 atoms and their associated hydrogens go to one side, and the other half go to the other side (Fig. 13a). Also along this plane, two O2-Fe bonds must be broken per (010) surface unit cell. One effect of the H atom on the O2 atoms is a weakening of the O2-Fe bonds which have lengths of 2.089 Å and 2.088 Å, whereas the O1-Fe bonds are stronger with lengths of 1.952 Å and 1.948 Å (Forsyth et al. 1968). Just from this,
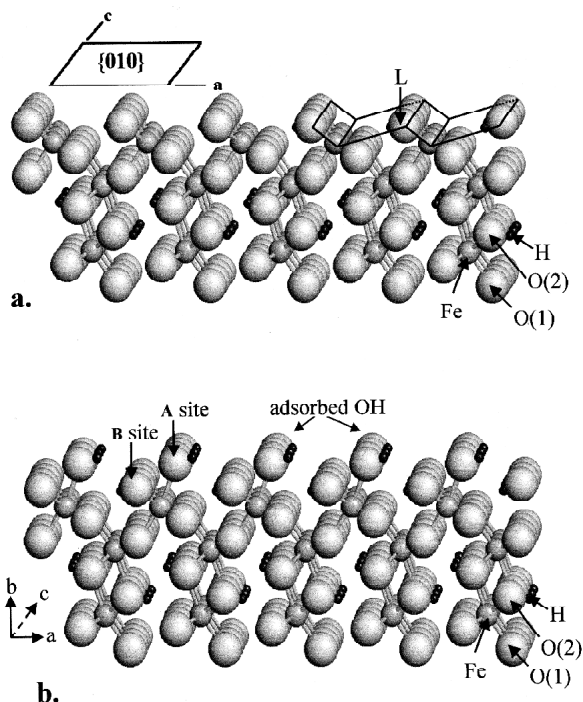

FIGURE 13. (a) Schematic of a fresh (010) cleavage surface in perspective. The corrugated plane labeled L indicates the feature shown in Figure 14. **(b)** The same surface after dissociative adsorption of H_2O. A sites are OH groups bound to one Fe atom and B sites OH groups bound to two Fe atoms.

one might expect that cleavage along the plane between the O2 atoms would be preferable relative to the plane between the O1 atoms. The modeling results presented next help quantify this notion.

Modeling results. The results from both the procrystal and Crystal95 models strongly support the notion that the (010) surface is defined by the O2 plane of hydroxylated O atoms. The procrystal model allows for the summing of electron density of critical points per unit area, and this was calculated for the two possible (010) cleavage planes discussed above so that the relative propensity for breakage between them could be directly compared. The electron density along the plane between staggered O1 atoms at 1/2 *b* is 1.128 e/Å^3 per surface unit cell, but only 0.819 e/Å^3 per (010) surface unit cell along the plane between staggered O2 atoms at 1/4 *b*, a decrease of 29%. Lower electron density equates to weaker bonds and easier breakage. Furthermore, surface energies calculated via the Crystal95 model show that the unrelaxed (010) surface terminated by O1 atoms at 1/2 *b* has a surface energy of 1.96 eV per surface unit cell (0.141 eV/Å^2), but the unrelaxed (010) surface terminated by O2 atoms at 1/4 *b* has an energy of only 1.52 eV per surface unit cell (0.110 eV/Å^2), a decrease of 28%. Therefore, the O2 surface is predicted to be more stable, again suggesting that the (010) surface is terminated with O2 atoms.

The corrugated surface exposed by cleavage along the plane between staggered O2 atoms is shown in Figure 13a. This outermost surface is characterized by rows of bidentate O2 atoms, followed by rows of Fe atoms with five coordinating O atoms
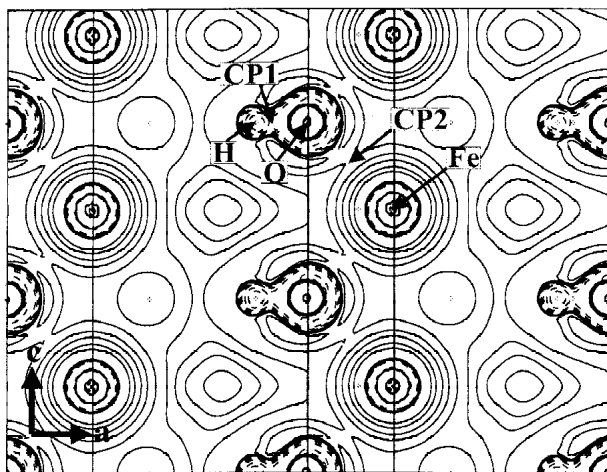
FIGURE 14. Contour map of the Laplacian of the charge density of a corrugated plane that connects the hydroxylated O2 atoms at the surface with the Fe atoms to which they are bonded (see Fig. 13a). The vertical lines indicate where the respective subplanes are tilted (see Fig. 13). Some of the atoms are labeled "O" (for oxygen), "H" (for hydrogen), "Fe" (for iron). Two of the (3,–1) critical points of the charge density are marked (CP1 for the critical point of the O-H bond, CP2 for the critical point of the Fe-O bond). See text for details.

(three O1 atoms and two O2 atoms), and rows of tridentate O1 atoms. Figure 14 shows the Laplacian of the charge density along this corrugated surface as calculated by Crystal95. Laplacian maps show where electronic charge is locally concentrated or depleted (Bader et al. 1984). The figure illustrates the bonding character of the goethite surface and the sites for possible nucleophilic and electrophilic attack. The O-H bond has a significant covalent character as illustrated by negative (dashed) contour lines of the Laplacian going around both the H and O atoms. These dashed contour lines indicate local "sinks" of the Laplacian, that is areas of high electron density where an electrophilic attack can occur. The (3,–1) critical point of the O-H bond is labeled CP1 in the figure. Solid lines, as around the Fe atoms, indicate local maxima of the Laplacian, that is areas of low electron density where a nucleophilic attack can occur. The (3,–1) critical point of the charge density along the Fe-O bond (CP2 in Fig. 14) separates almost perfect spheres of the negative Laplacian around O and the positive Laplacian around Fe indicating a bond of predominantly ionic character.

A new model for the (010) goethite surface. Traditionally, the O1 termination of the (010) surface has been used for reactivity modeling on goethite (Rochester and Topham 1979; Manceau and Charlet 1994; Barrón et al. 1996; Rustad et al. 1996a; 1996b). From the discussion above, however, it is apparent that this termination on (010) is unlikely relative to the termination on the O2 plane. Furthermore, the fivefold-coordinated iron on the O2 terminated surface most likely regains its octahedral coordination by adding a hydroxyl, so that the surface is now fully hydroxylated (Fig. 13b). Support for this model comes from IR spectroscopy (Rochester and Topham 1978) and the XPS results presented above that suggests a hydroxyl-rich surface. In addition Kurtz and Henrich (1987) have shown, using ultra-violet photoelectron spectroscopy (UPS), that H_2O molecules can dissociate on iron oxide surfaces resulting in surface functional hydroxyl groups.

The fully hydroxylated (010) surface, just described, involving O2 atoms results in rows of hydroxyls bonded to one iron atom (A sites) alternating with rows of hydroxyls bonded to two Fe atoms (B sites). On the O1 terminated (010) surface assumed in other studies, if it were to exist and assuming that all surface O atoms become hydroxylated, the same proportion (50–50) and distribution of hydroxylated A and B sites exist as on the O2 terminated terraces. In addition, the number and type of sites on a one unit-cell high step face (approximately 10 Å high like those shown in Fig. 6) are the same. However, the site distribution on the step face is different. For the unit-cell high step on the O2 terminated surface, there are A sites at the top edge of the step and also near the base of the step.

CONCLUSIONS

The microtopography of goethite growth surfaces can be, and often is, exceptionally complex. This microtopography is quite variable from sample to sample, and it may even be so on the same crystallographic face from the same sample. Because microtopography is often important, or even critical, in surface reactivity, various goethite samples may differ in reaction characteristics based on this alone.

Splitting the larger crystals used in this study may result in either the exposure of a buried growth surface or a fresh virgin cleavage (or other breakage) surface. The reaction potential of these two face types may be quite different. In addition, as seen in this study, buried growth surfaces are often accompanied by secondary phases. Aged vs. fresh surfaces (i.e., growth vs. virgin surfaces), as well as the exposure of secondary phases, may confuse the results of experiments run using ground powders.

The Laplacian map of the (010) surface terminated at $1/4$ b shows a concentration of electronic charge around the hydroxylated O2, allowing for Lewis acid character of this hydroxyl that is projecting from the surface. The surface Fe site is electronically depleted, but this is expected as one O2 is pulled away from each iron as a result of the cleavage process. This under-coordinated state is probably very short lived. From the several lines of evidence given above, the site is probably quickly rehydroxylated in the presence of air or water.

The two unique A sites on the face of unit-cell high steps on (010) surfaces may be particularly active in driving various reactions that occur on goethite surfaces due to their positions as described above. Steps are often particularly important in the overall reactivity of a mineral surface (e.g., Hochella 1990 and Junta and Hochella 1994) due to sites like these.

REFERENCES CITED

Allen G.C., Curtis, M.T., Hooper, A.J., and Tucker, P.M. (1974) X-ray photoelectron spectroscopy of iron-oxygen systems. Journal of the Chemical Society Dalton Transactions, 14, 1525–1530.

Bader, R.F.W. (1990) Atoms in Molecules A Quantum Theory, 438 p. Clarendon Press, Oxford.

Bader, R.F.W., MacDougall P.J., and Lau C.D.H. (1984) Bonded and nonbonded charge concentrations and their relation to molecular geometry and reactivity. Journal of the American Chemical Society, 106, 1594–1605.

Barrón V. and Torrent, J. (1996) Surface hydroxyl configuration of various crystal faces of hematite and goethite. Journal of Colloid and Interface Science, 177, 407–410.

Barrón, V., Galvez, N., Hochella, M.F., Jr., and Torrent, J. (1997) Epitaxial overgrowth of goethite on hematite synthesized in phosphate media: a scanning force transmission electron microscopy study. American Mineralogist, 82, 1091–1100.

Becker, U. and Hochella, M.F., Jr. (1996) The calculation of STM images, STS spectra, and XPS peak shifts for galena; new tools for understanding mineral surface chemistry. Geochimica et Cosmochimica Acta, 60, 2413–2426.

Becker, U., Hochella, M.F., Jr., and Aprá, E. (1996) The electronic structure of hematite {001} surfaces: Applications to the interpretation of STM images and heterogeneous surface reactions. American Mineralogist, 81, 1301–1314.

Brundle, C.R., Chuang, T.J., and Wandelt, K. (1977) Core and valence level photoemission studies of iron oxide surfaces and the oxidation of iron. Surface Science, 68, 459–468.

Clementi, E. and Roetti, C. (1974) Roothan-Hartree-Fock atomic wave functions. Atomic Data and Nuclear Data Tables, 14, 177–478.

Cornell, R.M. and Schwertmann, U. (1996) The iron oxides: Structure, Properties, Reactions, Occurrence and Uses, 573 p. VHC, New York.

Dovesi, R., Roetti, C., Freyria-Fava, C., Apra, E., Saunders, V.R., and Harrison, N.M. (1992) Ab initio Hartree-Fock treatment of ionic and semi-ionic compounds: state of the art. Philosophical Transactions of the Royal Society of London, A 341, 203.

Dovesi, R., Saunders, V.R., Roetti, C., Causa, M., Harrison, N.M., Orlando, R., and Apra, E. (1996) CRYSTAL95 User's Manual. University of Torino, Torino.

Downs, R.T., Andelman, A., and Hudacsko, M. (1996) The coordination numbers of Na and K in low albite and microcline as determined from a procrystal electron dencity distribution. American Mineralogist, 81, 1344–1349.

Eggleston, C.M. and Hochella, M.F., Jr. (1992) The structure of hematite {001} surfaces by scanning tunneling microscopy; image interpretation, surface relaxation, and step structure. American Mineralogist, 77, 911–922.

Fischer, L., Zur Mühlen, E., Brümmer, G.W., and Niehus, H. (1996) Atomic force microscopy (AFM) investigations of the surface topography of a multidomain porous goethite. European Journal of Soil Science, 47, 329–334.

Forsyth, J.B., Hedley, I.G., and Johnson, C.E. (1968) The magnetic structure and hyperfine field of goethite (α-FeOOH). Journal of Physics C, 1, 179–188.

Gibbs, G.V., Spackman, M.A., and Boisen, M.B. (1992) Bonded and promolecule radii for molecules and crystals. American Mineralogist, 77, 741–750.

Gibbs, G.V., Boisen, M.B., Hill, F.C., Osamu, T., and Downs, R.T. (1998) SiO and GeO bonded interactions as inferred from the bond critical point properties of electron density distributions. Physics and Chemistry of Minerals, 25, 574–584.

Gupta, R.P. and Sen, S. (1974) Calculation of multiplet structure of core p-vacancy levels. Physical Review B, 10, 71–77.

Hartman, P. and Perdok, W.G. (1953) On the relations between structure and morphology of crystals I. Acta Crystallogrphica, 8, 49–52.

Harvey, D.T. and Linton, R.W. (1981) Chemical characterization of hydrous ferric oxides by X-ray photoelectron spectroscopy. Analytical Chemistry, 53, 1684–1688.

Hays, K.F., Roe, A.L., Brown, G.E. Jr., Hodgson, K.O., Leckie, J.O., and Parks, G.A. (1987) In situ x-ray absoption study of surface complexes: Selenium oxyanios on α-FeOOH. Science, 238, 783–786.

Hochella, M.F. (1988) Auger and x-ray photoelectron spectroscopies. In Mineralogical Society of America Reviews in Mineralogy, 18, p. 573–637.

——(1990) Atomic structure, microtopography, composition, and reactivity of mineral surfaces. In Mineralogical Society of America Reviews in Mineralogy , 23, 87–132.

Hochella, M.F., Jr. and Carim, A.H. (1988a) A reassessment of electron escape depths in silicon and thermally grown silicon dioxide thin films. Surface Science, 197, L260–268.

Hochella, M.F., Jr., Eggleston. C.M., Elings. V.B., Parks, G.A., Brown, G.E., Jr., Wu, C.M., and Kjoller K. (1989) Mineralogy in two dimesions: Scanning tunneling microscopy of semiconducting minerals with implications for geochemical reactivity. American Mineralogist, 74, 1233–1246.

Junta, J.L. and Hochella M.F., Jr. (1994) Manganese (II) oxidation at mineral surfaces: A microscopic and spectroscopic study. Geochimica et Cosmochimica Acta, 58, 4985–4999.

Junta-Rosso, J. and Hochella, M.F., Jr. (1996) The chemistry of hematite {001} surfaces. Geochimica et Cosmochimica Acta, 60, 305–313.

Junta-Rosso, J., Hochella M.F., Jr., and Rimstidt, D. (1997) Linking microscopic and macroscopic data for heterogeneous reactions illustrated by the oxidation of manganese(II) at mineral surfaces. Geochimica et Cosmochimica Acta, 61, 149–159.

Kurtz, R.L. and Henrich, V.E. (1987) Surface electronic structure and chemisorption on corundum transition-metal oxides: α-Fe$_2$O$_3$. Physical Review B, 36, 3413–3421.

Leland, J.K. and Bard, A.J. (1987) Photochemistry of colloidal semiconducting iron oxide polymorphs. Journal of Physical Chemistry, 91, 5076–5083.

Manceau, A. and Charlet, L. (1994) The mechanism of selenate adsorption on goethite and hydrous ferric oxide. Journal of Colloid and Interface Science, 168, 87–93.

McIntyre, N.S. and Zetaruk, D.G. (1977) X-ray photoelectron spectroscopic studies of iron oxides. Analytical Chemistry, 49, 1521–1529.

Parfitt, R.L., Russell, J.D., and Farmer, V.C. (1975) Confirmation of the surface structures of goethite (α-FeOOH) and phosphated goethite by infrared spectroscopy. Soil Science Society of America Proceedings, 39, 1082–1087.

Pisani, C., Dovesi, R., and Roetti, C. (1988) Hartree-Fock ab-initio treatment of crystalline systems, Lecture Notes in Chemistry. Springer Verlag, Heidelberg.

Pratt, A.R., Nesbitt, H.W., and Muir, I.J. (1994) Generation of acids in mine waist waters: Oxidative leaching of pyrrhotite in dilute H$_2$SO$_4$ solutions (pH 3.0). Geochimica et Cosmochimica Acta, 58, 5147–5160.

Rakovan, J. and Reeder, R.J. (1994) Differential incorporation of trace elements and dissymmetrization in apatite: The role of surface structure during growth. American Mineralogist, 79, 892–903.

——(1996) Intracrystalline Rare Earth Element distributions in apatite: Surface structural influences on zoning during Growth. Geochimica et Cosmochimica Acta, 60, 4435–4445.

Rochester, C.H. and Topham, S.A. (1979) Infrared study of surface hydroxyl groups on goethite. Journal of the Chemical Society Faraday Transactions, 75, 591–602.

Roedder, E. (1984) In Mineralogical Society of America Reviews in Mineralogy, 12.

Russell, J.D., Parfitt, R.L., Fraser, A.R., and Farmer V.C. (1974) Surface structure of gibbsite, goethite and phosphated goethite. Nature, 248, 220–221.

Russell, J.D., Paterson, E., Fraser, A.R., and Farmer V.C. (1975) Adsorption of carbon dioxide on goethite (α-FeOOH) surfaces, and its implications for anion adsorption. Journal of the Chemical Society Faraday Transactions, 71, 1623–1630.

Rustad, J.R., Felmy, A.R., and Hay, B.P. (1996a) Molecular statics calculations of proton binding to goethite surfaces: A new approach to estimation of stability constants for multisite surface complexation models. Geochimica et Cosmochimica Acta, 60, 1563–1576.

——(1996b) Molecular statics calculations for iron oxide and oxyhydroxide minerals: Toward a flexible model of the reactive mineral-water interface. Geochimica et Cosmochimica Acta, 60, 1553–1562.

Schwertmann, U. (1984) The double dehydroylation peak of goethite. Thermocimica Acta, 78, 39–46.

Schwertmann, U. and Cornell, R.M. (1991) Iron Oxides in the Laboratory, Preparation and Characterization, 137 p. VCH, New York.

Schwertmann, U. and Taylor, R.M. (1990) Iron Oxides. In Minerals in Soil Environments, Vol. 1. p. 379–439. Soil Science Society of America, Madison, Wisconsin.

Sposito, G. (1984) The surface chemistry of soils, 234 p. Oxford University Press, New York.

Stipp, S.L. and Hochella, M.F., Jr. (1991) Structure and bonding environments at the calcite surface as observed with X-ray photoelectron spectroscopy (XPS) and low energy electron diffraction (LEED). Geochimica et Cosmochimica Acta, 55, 1723–1736.

Stipp, S.L.S., Eggleston, C.M., and Nielsen, B.S. (1994) Calcite surface structure at microtopographic and molecular scales with atomic force microscopy (AFM). Geochimica et Cosmochimica Acta, 58, 3023–3033.

Sunagawa, I. (1987a) Surface microtopography of crystal faces. In Morphology of Crystals, Part A. p. 321–365. Terra, Tokyo.

——(1987b) Morphology of Minerals. In I. Sunagawa, Ed., Morphology of Crystals, Part B. p. 511–587. Terra, Tokyo.

Terpstra, R.A., Bennema, P., Hartman, P., Woensdregt, C.F., Perdok, W.G., and Senechal, M.L. (1986) F faces of apatite and its morphology: Theory and observation. Journal of Crystal Growth, 78, 468–478.

Weidler, P.G., Schwinn, T., and Guab, H.E. (1996) Vicinal faces on synthetic goethite observed by atomic force microscopy. Clays and Clay Minerals, 44, 437–442.

Welsh, I.D. and Sherwood, P.M.A. (1989) Photoemission and electronic structure of FeOOH: Distinguishing between oxide and oxyhydroxide. Physical Review B, 40, 6386–6392.

Yang, X. and Bodnar, R. (1994) Magmatic-hydrothermal evolution in the "bottoms" of porphyry copper systems: Evidence from silicate melt and aqueous fluid inclusions in granitoid intrusions in the Gyeongsang basin, Sout Korea. International Geology Review, 36, 608–628.